Received: 5 March 2020 | Revised: 12 August 2020 | Accepted: 13 August 2020

DOI: 10.1002/glia.23902

GLIA

WILEY

RESEARCH ARTICLE

Differential effects of integrase strand transfer inhibitors, elvitegravir and raltegravir, on oligodendrocyte maturation: A role for the integrated stress response

Lindsay M. Roth[1,2] | Bassam Zidane[1,2,3] | Lindsay Festa[1,2] | Raj Putatunda[1] | Micah Romer[1] | Hubert Monnerie[1] | Kelly L. Jordan-Sciutto[2] | Judith B. Grinspan[1]

[1]Department of Neurology, The Children's Hospital of Philadelphia, Philadelphia, Pennsylvania

[2]Department of Basic and Translational Sciences, School of Dental Medicine, University of Pennsylvania, Philadelphia, Pennsylvania

[3]Faculty of Dentistry, King Abdulaziz University, Jeddah, Saudi Arabia

Correspondence
Kelly L. Jordan-Sciutto Department of Basic and Translational Sciences, School of Dental Medicine, University of Pennsylvania, 240 S 40th St, Philadelphia, PA 19104.
Email: jordank@upenn.edu

Judith B. Grinspan Department of Neurology, The Children's Hospital of Philadelphia, 516D Abramson Center, 3615 Civic Center Blvd, Philadelphia, PA 19104.
Email: grinspan@email.chop.edu

Funding information
Cellular Neuroscience Core of the Institutional Intellectual and Developmental Disabilities Research Core of the Children's Hospital of Philadelphia, Grant/Award Number: HD26979; Office of AIDS Research, Grant/Award Numbers: R21 MH118121, RO1 MH098742, T32 AI007632, T32 GM008076

Abstract

Regardless of adherence to combined antiretroviral therapy, white matter and myelin pathologies persist in patients with HIV-associated neurocognitive disorders, a spectrum of cognitive, motor, and behavioral impairments. We hypothesized that antiretroviral therapy alters the maturation of oligodendrocytes which synthesize myelin. We tested whether specific frontline integrase strand transfer inhibitors would alter oligodendrocyte differentiation and myelination. To model the effect of antiretrovirals on oligodendrocytes, we stimulated primary rat oligodendrocyte precursor cells to differentiate into mature oligodendrocytes in vitro in the presence of therapeutically relevant concentrations of elvitegravir or raltegravir and then assessed differentiation with lineage specific markers. To examine the effect of antiretrovirals on myelination, we treated mice with the demyelinating compound cuprizone, for 5 weeks. This was followed by 3 weeks of recovery in absence of cuprizone, during which time some mice received a daily intrajugular injection of elvitegravir. Brains were harvested, sectioned and processed by immunohistochemistry to examine oligodendrocyte maturation and myelination. Elvitegravir inhibited oligodendrocyte differentiation in vitro in a concentration-dependent manner, while raltegravir had no effect. Following cuprizone demyelination, administration of elvitegravir to adult mice reduced remyelination compared with control animals. Elvitegravir treatment activated the integrated stress response in oligodendrocytes in vitro, an effect which was completely blocked by pretreatment with the integrated stress response inhibitor Trans-ISRIB, preventing elvitegravir-mediated inhibition of oligodendrocyte maturation. These studies demonstrate that elvitegravir impairs oligodendrocyte maturation and remyelination and that the integrated stress response mediates this effect and may be a possible therapeutic target.

KEYWORDS

HAND, HIV, integrated stress response, myelin, neuroinflammation, oligodendrocytes

1 | INTRODUCTION

Despite effective viral suppression from combined antiretroviral (ARV) therapies (cART), approximately 50% of HIV-positive patients present with cognitive, motor, and behavioral impairments collectively termed HIV-associated neurocognitive disorders (HAND) (Heaton et al., 2011; Saylor et al., 2016). In the post cART era, pathological manifestations of HAND include persistent microgliosis, astrogliosis,

neuronal damage, synaptic loss and white matter abnormalities (Saylor et al., 2016; Shah et al., 2016). White matter changes include robust thinning of the corpus callosum, and loss of structural integrity and volume (Pomara, Crandall, Choi, Johnson, & Lim, 2001; Tate et al., 2011; Wohlschlaeger, Wenger, Mehraein, & Weis, 2009). Notably, severity of cognitive impairment has been correlated with amount of white matter damage, which increases with the length of time on cART (Jernigan et al., 2011). Furthermore, recent transcriptome analyses of individuals with HAND on ARV compounds identified dysregulated genes critical to oligodendrocyte maturation and myelination, such as myelin-associated glycoprotein, myelin oligodendrocyte glycoprotein, myelin basic protein (MBP) and oligodendrocyte transcription factor 1 (Borjabad et al., 2011; Solomon et al., 2019). Together, these findings suggest that white matter abnormalities persist despite cART adherence.

In the central nervous system (CNS), myelin is synthesized by oligodendrocytes whose lipid-enriched membrane is essential for the rapid transmission of action potentials and axonal trophic support (Waxman, 1980; Yin et al., 2006). Thus, myelin loss can contribute to neurocognitive dysfunction; however, the mechanism(s) underlying these changes remain unclear (Chen, Gill, & Kolson, 2014; Saylor et al., 2016). Although cART suppresses viral replication to undetectable levels in the periphery, inflammation and viral reservoirs still exist in the CNS (Finzi et al., 1997; Saylor et al., 2016). Additionally, ARV compounds themselves may contribute to the pathogenesis of HAND (Shah et al., 2016) and can induce toxicity in primary rat cortical neurons (Akay et al., 2014; Gannon et al., 2017; Robertson, Liner, & Meeker, 2012; Stern et al., 2018). One mediator of this ARV-induced toxicity is the integrated stress response (ISR) which is activated in neurons and astrocytes of HAND patients (Akay et al., 2012; Lindl, Akay, Wang, White, & Jordan-Sciutto, 2007). Transcriptome analysis of brain tissue from individuals with HAND on ARV compounds identified an upregulation of ISR genes such as activating transcription factor 4 (ATF4) (Solomon et al., 2019). The ISR is a cytoprotective mechanism which is activated in response to stressors including viral infections. However, if the stress is unresolved, cell death ensues (Pakos-Zebrucka et al., 2016; Romero-Ramírez, Nieto-Sampedro, & Barreda-Manso, 2017). We previously reported that ARV compounds from the protease inhibitor class ritonavir, lopinavir, saquinavir and darunavir, inhibited oligodendrocyte maturation, in vitro, while ritonavir also inhibited myelin protein production, in vivo (Festa et al., 2019; Jensen et al., 2015).

In the present study, we tested a new class of ARV compounds, integrase strand transfer inhibitors (INSTIs), which inhibit the function of the HIV integrase enzyme which integrates the reverse transcribed viral DNA into the host cell genome (Arts & Hazuda, 2012; Deeks, 2014). All current frontline cART regimens include one INSTI, making these compounds clinically relevant to study (AIDSinfo, 2019; WHO, 2016). We demonstrate that elvitegravir (EVG), but not raltegravir (RAL), decreased oligodendrocyte maturation, in vitro, and inhibited remyelination following cuprizone-mediated demyelination, in vivo (Matsushima & Morell, 2001). Finally, we show that the ISR mediates the effects of EVG in our in vitro oligodendrocyte maturation model. Our results suggest that EVG could contribute to myelin abnormalities seen in HAND patients and provides further evidence to suggest the ISR could be therapeutically relevant to these patients.

2 | MATERIAL AND METHODS

Animal use: All experiments were performed in accordance with the guidelines set forth by The Children's Hospital of Philadelphia and The University of Pennsylvania Institutional Animal Care and Use Committees.

Preparation of primary rat oligodendrocyte precursor cell cultures. Primary rat oligodendrocyte precursor cells (OPCs) were isolated from brains of postnatal day 1 Sprague Dawley rats (Charles River Laboratories, Wilmington, MA RRID: RGD_737891) and plated on T75 flasks as previously described (Jensen et al., 2015). OPCs were then purified (>90%) using the "shake-off" method (McCarthy & de Vellis, 1980).

Drug treatments. OPCs were grown in 24-well plates with coverslips or 10 cm tissue culture dishes, for immunocytochemistry and immunoblotting, respectively, until they reached about 70% confluency. To differentiate the cells into mature oligodendrocytes, growth medium was replaced with differentiation medium prepared as previous described (Feigenson, Reid, See, Crenshaw, & Grinspan, 2009). The cells were treated with vehicle (DMSO or PBS), EVG (350 nM, 3.5 μM or 10 μM), RAL (300 nM, 3.0 μM or 10 μM) or cobicistat, an INSTI booster (COBI; 150 nM, 1.5 μM, 4 μM) for 72 hr, to allow differentiation to occur before immunolabeling or protein collection. Pretreatment with Trans-ISRIB (5 μM) was administered 1 hr prior to EVG (3.5 μM or 10 μM) exposure.

Immunofluorescence. Cells were prepared and stained with propidium iodide and A2B5 or galactocerebroside (GalC) and MBP as previously described (Festa et al., 2019). Primary antibodies used were: A2B5 for OPCs (1:1 dilution, mouse IgM hybridoma) (Eisenbarth, Walsh, & Nirenberg, 1979); GalC for immature oligodendrocytes (1:5 dilution, mouse IgG hybridoma) (Raff, Mirsky, Fields, & Nature, 1978); myelin basic protein (MBP) for mature oligodendrocytes (1:1 dilution, rat hybridoma courtesy of Dr. Virginia Lee, University of Pennsylvania). Secondary goat anti-mouse antibodies were applied for 30 minutes at room temperature, except for MBP which was incubated with goat anti-rat secondary (1:200, Jackson ImmunoResearch RRID: SCR_010488). Cells were imaged at 40x magnification using a Keyence BZ-X-700 digital fluorescent microscope (Keyence Corporation, Itasca, IL RRID:SCR_016979) and were hand-counted using Fiji (NIH RRID: SCR_002285) to quantify the number of OPCs, immature and mature oligodendrocytes. Averages were calculated across 20 fields/coverslip with 2–4 coverslips per condition for each biological replicate.

TUNEL assay. To determine whether cells were undergoing apoptotic cell death, a TUNEL staining protocol was performed as previously described (Gavrieli, Sherman, & Ben-Sasson, 1992).

RNA extraction and qPCR. The expression of MBP in oligodendrocyte cultures was quantified using quantitative reverse transcription

polymerase chain reaction (qPCR). RNA isolation and cDNA preparation were performed as previously described (Jensen et al., 2015). qPCR was performed using Power SYBR Green, as previously described (Feigenson et al., 2009). Samples were measured in triplicate for each experiment from 3 biological replicates. Data were normalized using Protein Kinase Gene 1 and were analyzed according to the comparative threshold (ΔΔCT) cycle method. Primer pairs for MBP obtained from Integrated DNA Technologies (Coralville, IA). Forward: 5′-TGA AAA CCC AGT CCA C- 3′. Reverse: 5′- GGA TTA AGA GAG GGT CGT C-3′.

Nuclear/Cytoplasmic fractionation. For examination of ATF4 levels, nuclear/cytoplasmic fractionation was performed as previously described (Gannon et al., 2017).

Immunoblotting. Protein lysates were collected and probed for proteins of interest as previously described (Festa et al., 2019). Primary antibodies to the following antigens were used: MBP (SMI-99; 1:1000, Biolegend, Cat#: 808401, RRID: AB_2564741), proteolipid protein (PLP; 1:1000, rat hybridoma); alpha tubulin (α-tubulin; 1:10,000, Sigma, Cat#: T5168, RRID: AB_477579), activating transcription factor 4 (ATF4; 1:1000, ProteinTech, Cat#: 10835-1-AP, RRID: AB_2058600), phosphorylated eukaryotic initiation factor 2 alpha (pEIF2α; 1:1000, Cell Signaling, Cat#: 9721, RRID: AB_330951), total eukaryotic initiation factor 2 alpha (tEIF2α; 1:1000, Cell Signaling, Cat#: 2103, RRID:AB_836874), Lamin B1 (1:1000, ProteinTech, Ca#: 12987-1-AP, RRID: AB_213690) and glyceraldehyde 3-phosphate dehydrogenase (GAPDH; 1:8000, Sigma, Cat# MAB374 RRID: AB_2107445). Membranes were incubated with specific fluorescent probe-conjugated secondary antibodies (1:10,000, LI-COR Biosciences) including goat anti-mouse IRdye 800CW (Cat# 926–32,212, RRID:AB_621847), goat anti-mouse IRdye 680RD (Cat# 925–68,070, RRID:AB_2651128), goat anti-rat IRdye 680RD (Cat# 926–32,229, RRID:AB_1850020) and goat anti-rabbit IRdye 680RD (Cat# 926–68,071, RRID:AB_10956166) diluted in Tris-buffered saline/tween-20 + 5% bovine serum albumin (BSA). Membranes were visualized and analyzed using an Odyssey Infrared Imaging System (LI-COR Biosciences, RRID:SCR_013430). ATF4 blots were probed with rabbit-specific horseradish peroxidase-conjugated secondary antibodies (1:40,000; GE Healthcare) and subsequently incubated with SuperSignal West Dura (Thermo Scientific) then exposed to X-ray film for 1 min. Densitometric analysis of band intensities was conducted by Fiji (NIH RRID: SCR_002285). All bands were normalized to the loading control, as specified in each experiment.

Mass spectrometry study. C57BL/6 female mice 6–8 weeks old (Jackson Laboratories, PA) were used to determine the maximum plasma concentration of EVG via mass spectrometry. Twenty mice (five/group) were implanted with I.V. cannula into the jugular vein and received a single dose of EVG/COBI. Blood was collected via the submandibular vein after 3 hr and processed for mass spectrometry analysis. For the implantation of the cannulas, sustained release buprenorphine (0.5–1.0 mg/kg) was administered by subcutaneous injection before the start of surgery. A ketamine/xylazine cocktail (80 and 12 mg/kg, respectively) was used to anesthetize the mice. A silastic I.V. cannula was inserted into the jugular vein, sutured in place using PERMA-HAND silk suture and mounted on the back of the mouse using a mesh back-mount.

Cuprizone model and in-vivo *drug treatments*. C57BL/6 female mice 6–8 weeks old were used for the cuprizone demyelination model and were divided into two groups: control (powdered chow) and cuprizone in powdered chow (0.25%). Each group was then subdivided into untreated, vehicle (DMSO), EVG/COBI-treated, with three mice per group for a total of 24 animals. After 5 weeks of cuprizone feeding, three control mice and three cuprizone mice were perfused, their brains removed and prepared for frozen sections (see below) to determine the extent of the cuprizone lesion. The other mice were implanted with I.V. cannulas into the jugular vein, as described above, and injected once daily with either DMSO (5%) or EVG/COBI (65 mg/kg, diluted in 5% DMSO), while being fed a conventional diet during the last 3 weeks of the experiment (recovery period).

Immunohistochemistry. Mice were anesthetized with a ketamine/xylazine cocktail and intracardially perfused with cold PBS, then 4% paraformaldehyde (pH 7.4). Whole brains were postfixed in 4% paraformaldehyde for 2 hr and then immersed in 30% sucrose solution for at least 24 hr. Brains were cryopreserved in optimal cutting temperature compound (OCT) and then coronally sectioned at 12 μm on a cryostat (Leica Microsystems, Exton, PA) throughout the entire corpus callosum, collecting three sections per slide. The third ventricle was used as a regional anatomical marker for the region of the corpus callosum most consistently demyelinated by cuprizone ingestion. These sections were labeled overnight at 4°C with: anti-aspartoacylase (ASPA; 1:500, GeneTex, Cat# GTX110699, RRID:AB_2036282) (Madhavarao et al., 2004) to detect mature oligodendrocytes; anti-neural/glial antigen 2 (NG2; 1:200, Millipore, Cat# AB5320, RRID: AB_11213678) to detect OPCs; anti-Ionized calcium binding adaptor molecule 1 (IBA1; 1:500, Wako, Cat# 019–19,741, RRID:AB_839504) to detect microglia and anti-glial fibrillary acidic protein (GFAP; 1:2, hybridoma supernatant courtesy of Dr. Virginia Lee, University of Pennsylvania) to detect astrocytes. Secondary goat anti-rabbit antibodies were applied for 30 minutes at room temperature (1:200, Jackson ImmunoResearch, RRID:SCR_010488), except for GFAP which was incubated with goat anti-rat secondary (1:200, Jackson ImmunoResearch). All antibodies were diluted in PBS containing 20% FBS, 0.02% BSA, 0.001% Triton X-100 and 0.02% NaN_3. Sections were incubated for 20 minutes with FluoroMyelin green (1:500, ThermoFisher Scientific, Cat# F34651) diluted in PBS to confirm changes in myelination.

To quantify cell number or fluorescent intensity, brains from at least three mice were used per condition. Digital images were taken at 40X magnification from sections. Within the corpus callosum of each brain section from at least two sections per animal, five 150 cm X 150 cm regions of interest were used for counting cells positive for markers of interest or measured for mean fluorescent intensity using Fiji.

Luxol fast blue (LFB) staining. Sections were taken through 95% ethanol briefly, 0.1% LFB for 16–18 hr, 95% ethanol for 2 minutes, 0.05% lithium carbonate solution for 2 minutes, 70% ethanol for

30 seconds. After a quick rinse in water, the slides were incubated in 0.1% Cresyl violet for 11 minutes at 56°C. Finally, following washes with 95% ethanol and xylene, slides were sealed with coverslips using Permount. Following LFB staining, sections with the medial habenula present were used for semi-quantitative analysis. This anatomical marker validated that sections were from the region of the corpus callosum consistently demyelinated by cuprizone ingestion.

Statistical analysis. Statistical analysis was performed with GraphPad Prism software (version 7.0; RRID: SCR_002798). Cell cultures prepared from each litter represent independent biological replicates, which were treated with either vehicle or drug in the indicated concentrations. An untreated condition (UT), in which cells were placed in differentiation media only, was also included in each biological replicate, to which all data were normalized unless otherwise specified. The UT condition is graphically represented by a dotted line. Repeated measures analysis of variance (ANOVA) followed by Dunnett's post hoc (for in vitro analysis) or Tukey's post hoc (for in vivo analysis) was used to compare data while accounting for inherent correlations present within a single biological replicate. The significance level was $p < .05$.

3 | RESULTS

Elvitegravir inhibits oligodendrocyte maturation while raltegravir does not. We previously, reported that the protease inhibitors, ritonavir, lopinavir, saquinavir and darunavir, inhibited the maturation of oligodendrocytes, in vitro (Festa et al., 2019; Jensen et al., 2015). Using our well-established culture model, (Feigenson et al., 2009) we presently examined whether two INSTIs, EVG and RAL had similar effects. We based EVG and RAL concentrations on reported plasma and cerebrospinal fluid (CSF) levels in humans, since measurements in human brain parenchyma have not been performed (Podany, Scarsi, & Fletcher, 2017; Yilmaz et al., 2009).

Clinically, EVG is administered with cobicistat (COBI), a robust inhibitor of cytochrome p450, which metabolizes EVG (Deeks, 2014; Podany et al., 2017). By combining EVG with COBI, lower concentrations of EVG can be administered to patients, thus reducing side effects while achieving therapeutically relevant concentrations in the body. Although COBI is not an ARV compound, we also examined its effect on oligodendrocyte maturation in vitro because it was used in combination with EVG in our in vivo experiments. Purified OPCs were placed in differentiation medium and exposed to therapeutically relevant concentrations of EVG (350 nM, 3.5 μM, 10 μM), RAL (300 nM, 3 μM, 10 μM) or COBI (150 nM, 1.5 μM, 4 μM) for 72 hr. Then, cultures were immunostained for stage-specific oligodendrocyte markers: GalC and MBP for immature and mature oligodendrocytes, respectively (Raff et al., 1978). Representative images and counting analysis of drug-treated oligodendrocytes show many fewer GalC-positive cells in 3.5 and 10 μM EVG-treated cultures compared with controls (Figure 1a,b). The number of MBP-expressing oligodendrocytes was also significantly lower than controls following EVG treatment (Figure 1c). In contrast, neither RAL nor COBI affected oligodendrocyte differentiation, regardless of the concentration (Figure 1a–c). Additionally, we observed no differences in total cell number following treatment with EVG, RAL or COBI compared with controls (DAPI+; Figure 1d).

Elvitegravir does not induce cell death or alter OPC number. To assess whether there was an alteration in the number of OPCs or cell death to account for the changes in GalC-positive and MBP-positive cells observed in cultures exposed to EVG, we treated OPCs at the time of differentiation with EVG (3.5 μM, 10 μM) and stained for A2B5-positive OPCs (Figure 2a,c), propidium iodide-positive cells (Figure 2d) and cells positive for terminal UTP Nick end labeling (TUNEL) (Figure 2b,e), which stains double-stranded DNA breaks, one of the first processes in apoptotic cell death. After 72 hr of differentiation, the number of A2B5-positive cells did not change following EVG treatment (Figure 2c). As a positive control, OPCs not placed in differentiation media were also stained for A2B5. Since these cells continued to proliferate, there was a significant increase in A2B5-positive cells in the OPCs control compared with vehicle control (Figure 2c). There was no increase in the number of propidium iodide-positive cells or TUNEL-positive cells in EVG-treated cultures compared with controls (Figure 2d,e). DNase was used as a positive control for the TUNEL assay and it significantly increased TUNEL-positive cells compared with controls (Figure 2b,e). Together, these results suggest that EVG inhibits oligodendrocyte maturation by interfering with the differentiation process itself. Since EVG exposure significantly decreased the number of MBP-positive cells, we examined MBP *mRNA* levels. EVG (3.5 μM and 10 μM) resulted in significantly lower MBP *mRNA* levels compared with controls (Figure 2f).

Elvitegravir inhibits myelin protein production. Since EVG treatment decreased the number of MBP-positive cells and MBP *mRNA* expression, we examined whether these effects correlated with reduced myelin protein levels. The cultures were treated with EVG for 72 hr, cell extracts were collected, and protein lysates processed for immunoblot analysis. EVG (3.5 μM and 10 μM) treatment resulted in significantly lower levels of both MBP and PLP protein expression compared with controls (Figure 3a). In contrast, neither RAL nor COBI affected MBP protein expression (Figure 3b,c).

Elvitegravir-mediated inhibition of oligodendrocyte maturation is reversible. To determine whether the effect of EVG on OPC differentiation was permanent, we incubated the cells with 3.5 μM or 10 μM EVG for 72 hr in differentiation medium, then washed out the drug and added fresh differentiation medium for 24, 48, or 72 hr. As shown in Figure 4a,b, while 72-hr treatment with 3.5 μM EVG resulted in fewer GalC-positive cells compared with controls, removing 3.5 μM EVG significantly reversed this effect after 24, 48, and 72 hr. However, at 10 μM EVG there was no significant recovery at 24 or 48 hr and only a partial recovery was observed at 72 hr compared with controls (Figure 4a,b). The same effect was true for MBP-positive cells in which removing 3.5 μM EVG after 24, 48, and 72 hr significantly reversed its effect, while only a partial recovery occurred at 10 μM EVG (Figure 4c). Similarly, 24 hr in fresh differentiation medium following removal of 3.5 μM EVG increased MBP protein levels to control levels as detected by immunoblotting (Figure 4d). In contrast,

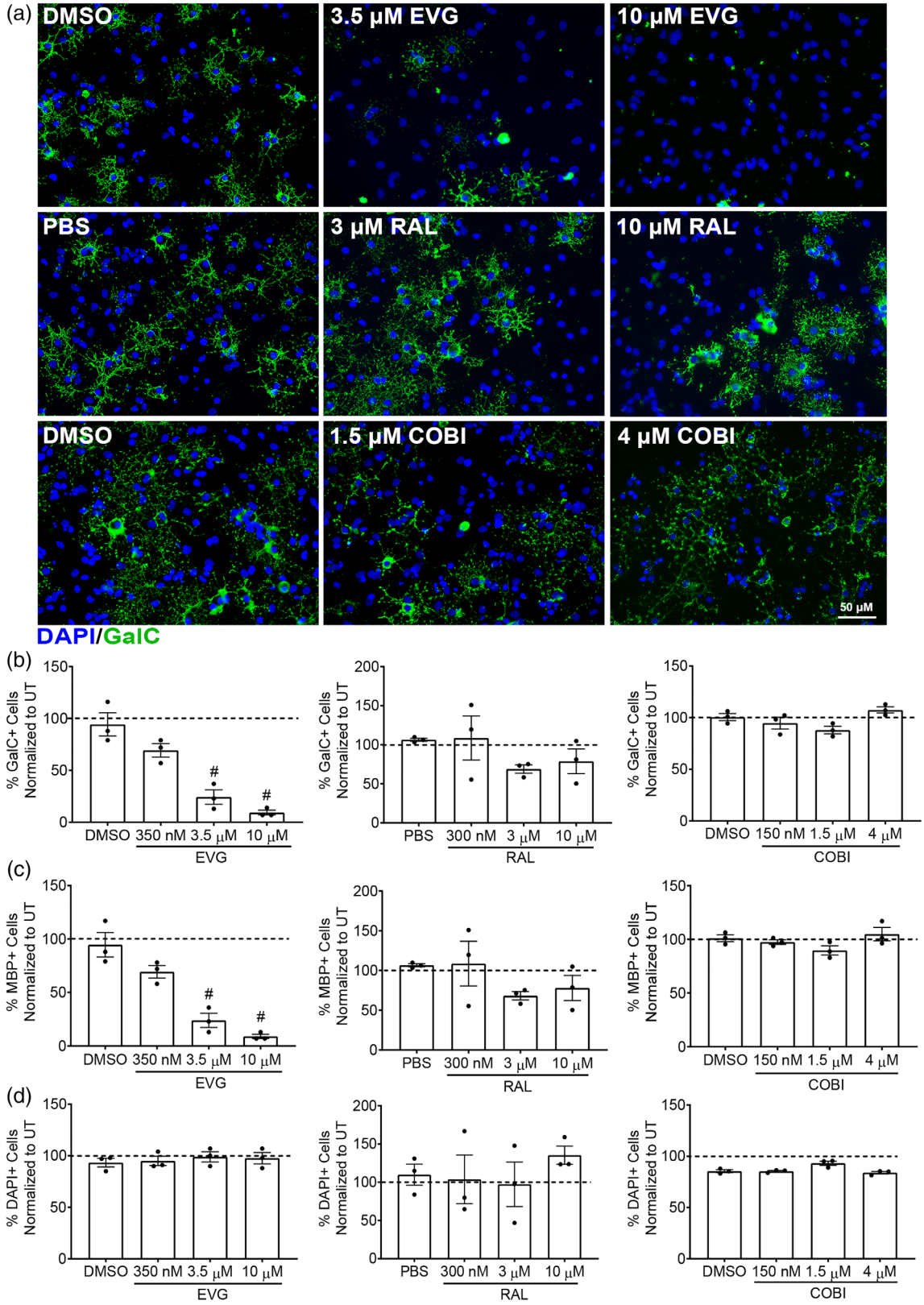

FIGURE 1 EVG inhibits oligodendrocyte differentiation but RAL nor COBI do not. (a) Representative photomicrographs of primary rat oligodendrocyte cultures grown in differentiation medium for 72 hr and treated with EVG, RAL or COBI and stained for GalC and DAPI; scale bar = 50 μm. (b) Quantification of GalC-positive immature oligodendrocytes normalized to the number of DAPI-positive cells and expressed as percent of untreated (UT). (c) Quantification of MBP-positive mature oligodendrocytes normalized to the number of DAPI-positive cells and expressed as a percent of UT. #$p < .05$ vs. vehicle (DMSO or PBS). (d) Quantification of DAPI-positive cells expressed as percent of UT [Color figure can be viewed at wileyonlinelibrary.com]

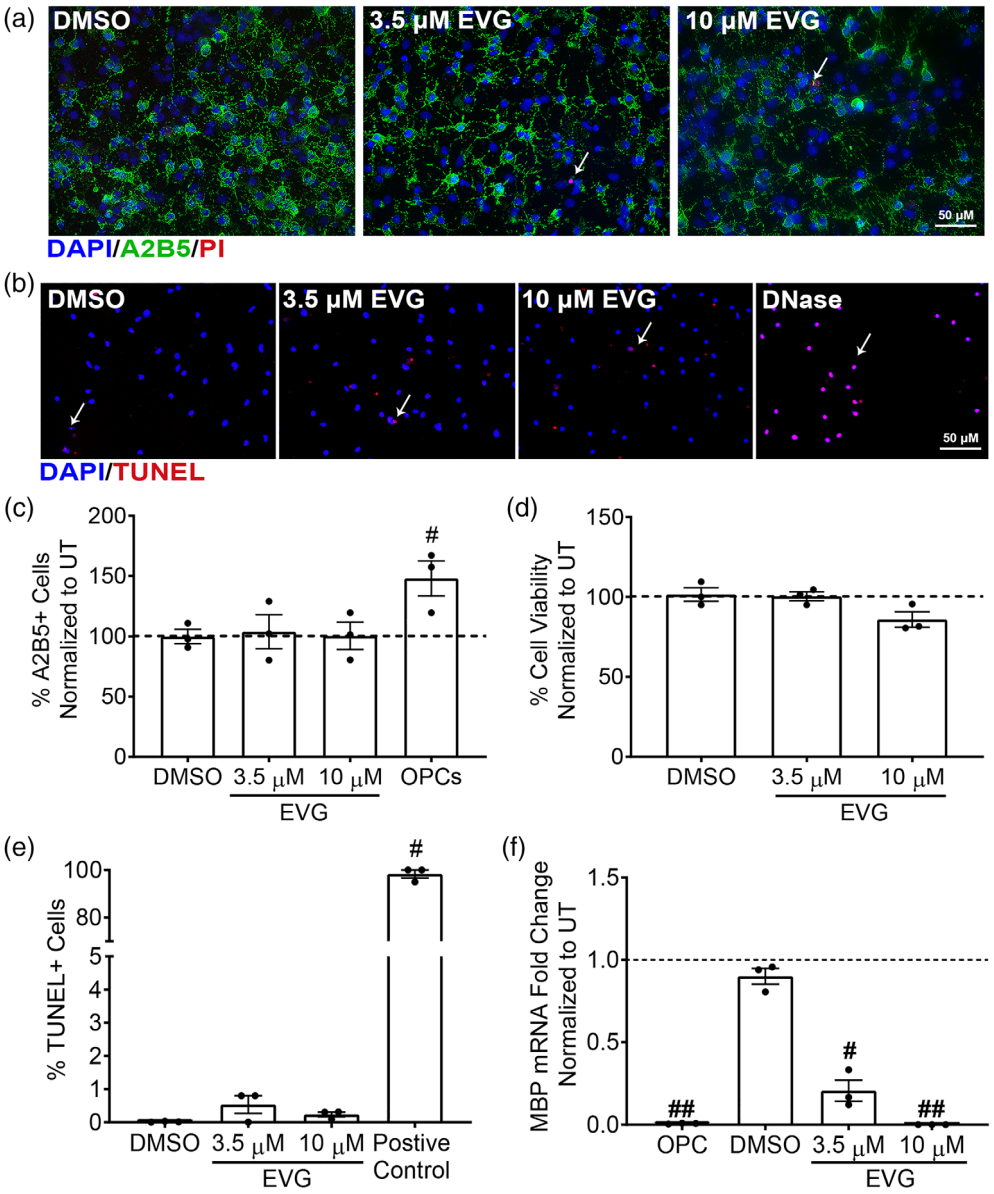

FIGURE 2 EVG does not alter OPC number or cause cell death. (a) Representative photomicrographs of primary rat oligodendrocyte cultures grown in differentiation medium for 72 hr and treated with EVG and stained for A2B5, propidium iodide (PI) and DAPI. Arrows point to PI-positive cells; scale bar = 50 μm. (b) Representative photomicrographs of primary rat oligodendrocyte cultures grown in differentiation medium for 72 hr and treated with EVG and stained for TUNEL and DAPI. Arrows point to TUNEL-positive cells; scale bar = 50 μm. (c) Quantification A2B5-positive OPCs normalized to the number of DAPI-positive cells, and expressed as a percent of UT. OPCs not placed in differentiation media were used as a positive control. d) Quantification of cell viability determined by the number of propidium iodide-negative cells normalized to the number of DAPI-positive cells, and expressed as a percent of UT. (e) Quantification of apoptotic cell death determined by the number of TUNEL-positive cells in each condition normalized to the number of DAPI-positive cells. DNase was used as a positive control. #$p < .0001$ vs. DMSO. (f) Quantification of MBP *mRNA* levels following treatment with EVG. Determination of MBP mRNA expression relative to that of UT. #$p < .05$, ##$p < .01$ vs. DMSO. All Graph data are expressed as mean ± *SEM* from three independently prepared cultures [Color figure can be viewed at wileyonlinelibrary.com]

24 hr after removal of 10 μM EVG, MBP protein levels remained low (Figure 4d). These data indicate that 3.5 μM EVG has a reversible effect on oligodendrocyte maturation, while higher doses may inflict more permanent damage.

Elvitegravir inhibits remyelination in a mouse model of cuprizone demyelination. To identify a dose of EVG comparable to plasma concentrations measured in patients taking EVG, we tested several doses of EVG up to 65 mg/kg, collected blood 3 hr after injection and examined plasma concentrations by mass spectrometry. The 65 mg/kg dose resulted in physiologically comparable maximum plasma concentrations of EVG measured in humans and thus was used for all in vivo experiments (Table 1).

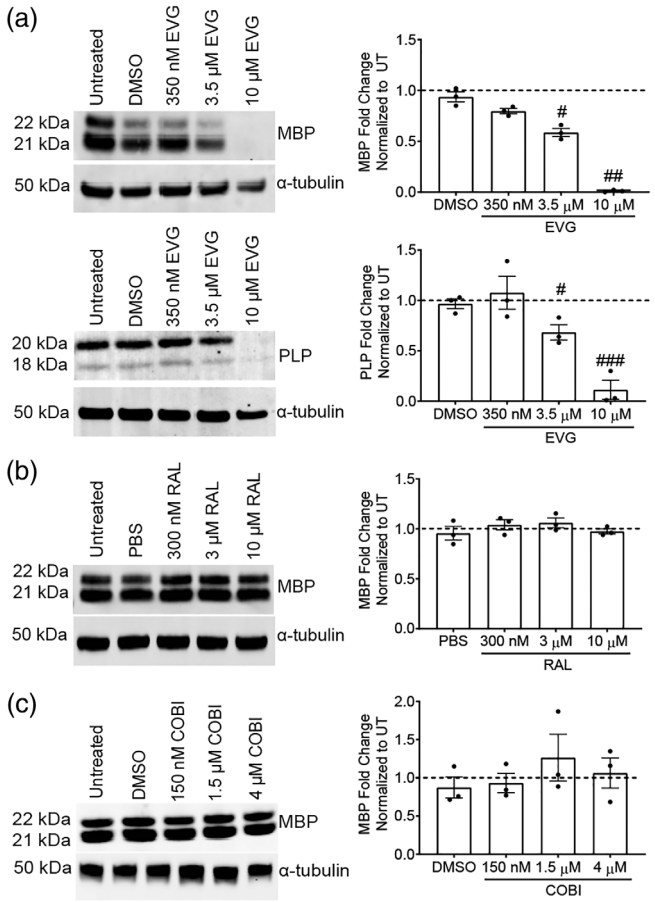

FIGURE 3 OPCs treated with EVG, but not RAL or COBI, express significantly less myelin protein (MBP and PLP) after differentiation than controls. Representative western blot images and quantifications of band intensities of MBP and/or PLP immunoreactivies from cultured oligodendrocytes exposed to various concentrations of EVG (a), RAL (b) or COBI (c) for 72 hr with α-tubulin as a loading control. Graph data are expressed as mean ± *SEM* from three independently prepared cultures. Protein band intensities normalized to α-tubulin are expressed as a fold change of UT. #*p* < .05, ##*p* < .01, ###*p* < .001 vs. vehicle (DMSO or PBS)

To examine the effect of EVG on remyelination, we used a widely implemented toxin-induced demyelination mouse model. The copper chelator bis-cyclohexanone-oxaldihydrazone (cuprizone) is combined into mouse feed for 5 weeks, and results in targeted demyelination in the corpus callosum, the largest white matter tract in the mouse brain (Matsushima & Morell, 2001). In addition to oligodendrocyte death, microglia and astrocytes accumulate at the lesion site (Matsushima & Morell, 2001). Removal of cuprizone from the feed after 5 weeks allows remyelination to occur over the course of three additional weeks (the recovery period) (Matsushima & Morell, 2001). EVG was administered daily via I.V. jugular vein cannula during the 3 week recovery period together with COBI as a bioavailability booster, while control animals received either the vehicle, DMSO or no injection (Figure 5a). Mouse brains were removed at 5 and 8 weeks, processed for frozen sections and stained with luxol fast blue (LFB) to label myelin (Figure 5b). The 5 week cuprizone-treated mice displayed a robust decrease in myelin in the medial corpus callosum, which was completely rescued following 3 weeks of recovery (Figure 5b). In contrast, at the end of the recovery period, EVG-injected cuprizone mice had significantly less myelin compared with untreated or DMSO-injected cuprizone mice (Figure 5b). Interestingly, there were no changes in myelin in EVG-injected control mice compared with the untreated or DMSO-injected control mice (Figure 5b,e). Quantification of LFB intensity by blinded scoring confirmed these differences (Figure 5e) (Yu et al., 2017). In order to further validate the changes in myelination observed in EVG-injected cuprizone mice, we immunostained sections with fluoromyelin green (Figure 5c). Fluoromyelin staining intensity was significantly decreased in EVG-injected cuprizone mice compared with DMSO-injected cuprizone control mice at the end of the recovery period (Figure 5c,f). Immunostaining for the mature oligodendrocyte marker ASPA showed significantly fewer ASPA-positive cells in the 5 week cuprizone mice compared with 5 week control mice as expected. After 3 weeks of recovery, the number of ASPA-positive cells in untreated cuprizone mice had increased to those of control mice (Figure 5d,g). However, ASPA-positive cells in EVG-injected cuprizone mice remained drastically reduced compared with any control mice (Figure 5d,g). These data indicate that EVG results in reduced levels of remyelination and fewer mature oligodendrocytes but does not reduce existing myelin in this experimental paradigm.

Elvitegravir treatment prolongs neuroinflammation following cuprizone-induced demyelination and causes accumulation of OPCs at lesion site. To examine the effects of EVG on the inflammatory environment during remyelination, we stained mouse brain sections for astrocytes and microglia using GFAP and IBA1, respectively. As expected, increased levels of GFAP and IBA1 staining intensity were observed in 5 week cuprizone mice which returned to normal after 3 weeks of recovery (Figure 6a,c). However, in EVG-injected cuprizone mice, both GFAP and IBA1 intensities remained elevated after 3 weeks of recovery (Figure 6a,c). EVG-injected control mice did not show changes in IBA1 or GFAP intensities compared with control mice.

Finally, to further validate the effect of EVG on oligodendrocyte differentiation in vivo, we stained mouse brain sections for OPCs using NG2. We observed an increase in NG2 intensity in 5 week cuprizone mice which returned to the levels observed in control mice after 3 weeks of recovery (Figure 6b,c). However, in EVG-injected cuprizone mice NG2 intensity remained elevated compared with untreated and DMSO-injected cuprizone mice (Figure 6b,c). EVG-injected control mice did not display increased NG2 staining intensity compared with untreated or DMSO-injected controls, consistent with intact myelin.

Elvitegravir activates the ISR in oligodendrocytes in vitro. Studies have shown that factors released by HIV-infected immune cells in the brain as well as ARV compounds (Finzi et al., 1997; Saylor et al., 2016) can activate the ISR, suggesting a role in HAND pathogenesis and/or persistence (Akay et al., 2012; Akay et al., 2014; Gannon et al., 2017; Lindl et al., 2007; Stern et al., 2018). ISR activation causes phosphorylation of eIF2α which attenuates global protein translation while

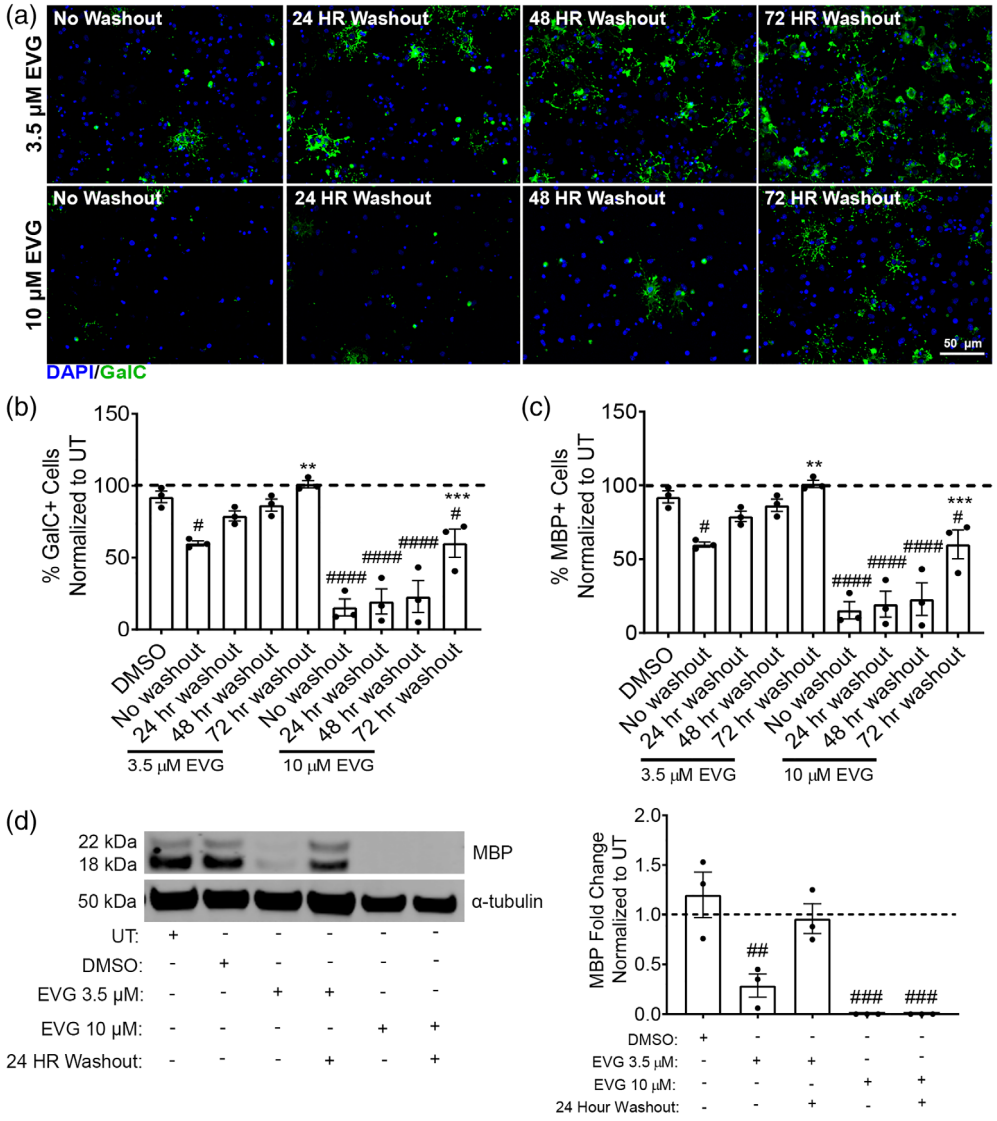

FIGURE 4 Elvitegravir-driven inhibition of oligodendrocyte differentiation is reversible. (a) Representative photomicrographs of primary rat oligodendrocyte cultures grown in differentiation medium for 72 hr with EVG. Cells were then replaced with fresh differentiation medium for an additional 24, 48 or 72 hr and stained for GalC and DAPI; scale bar = 50 μm. (b) Quantification of GalC-positive immature oligodendrocytes normalized to the number of DAPI-positive cells and expressed as percent of untreated (UT). (c) Quantification of MBP-positive mature oligodendrocytes normalized to the number of DAPI-positive cells and expressed as a percent of UT. #p < .05 vs. DMSO. Graph data are expressed as mean ± *SEM* from three independently prepared cultures. #p < .05, ##p < .01, ####p < .0001 vs. DMSO; **p < .01, ***p < .001, vs. No Washout. (d) Representative western blot image and quantification of band intensities of MBP immunoreactivity from cultured oligodendrocytes exposed to various EVG concentrations for 24 hr with α-tubulin as a loading control. Graph data are expressed as mean ± *SEM* from three independently prepared cultures. Protein band intensities normalized to α-tubulin are expressed as a fold change of UT.##p < .01, ###p < .001 vs. DMSO [Color figure can be viewed at wileyonlinelibrary.com]

TABLE 1 Comparison of maximum plasma concentration of elvitegravir in mice versus humans

	Mice		Humans[24,36]	
Drug	Average maximum plasma concentration (ng/ml)	Average maximum plasma concentration (μM)	Average maximum plasma concentration (ng/ml)	Average maximum plasma concentration (μM)
Elvitegravir	1945.32	4.34	1,550	3.46

promoting translation of certain stress response proteins including ATF4 (Pakos-Zebrucka et al., 2016; Romero-Ramírez et al., 2017). Since myelin synthesis requires massive production of lipids and proteins, it is unsurprising that the ISR has been implicated in numerous myelin disorders that share a common white matter pathology also observed in HAND (Clayton & Popko, 2016). However, it is not

known whether the ISR is specifically activated in oligodendrocytes or is involved in white matter pathologies persistent in HAND.

To this end, we examined whether EVG exposure activated the ISR in vitro. Cells were treated with EVG (3.5 or 10 μM) for 24, 48 or 72 hr before cell extracts were collected and processed for immunoblotting. In addition, nuclear and cytoplasmic fractionation was performed to examine nuclear ATF4 induction. Thapsigargin (THAP, 500 nM), a strong ISR enhancer (Gannon et al., 2017), was used as a positive control at 2 hr and 24 hr for pEIF2α and ATF4, respectively. We observed an increase in pEIF2α in 3.5 μM EVG-treated cultures after 72 hr, compared with controls. This effect was stronger at 10 μM EVG since pEIF2α levels were significantly increased at 48 and 72 hr compared with controls (Figure 7a-d). ATF4 expression was significantly increased in 10 μM EVG-treated cultures at all time points measured. While there was no change in ATF4 expression at 24 or 48 hr in 3.5 μM-EVG treated cultures compared with controls, ATF4 expression trended towards elevation at 96 hr, but was not statistically significant (Figure 7e-h).

The ISR partially mediates elvitegravir-driven inhibition of oligodendrocyte maturation, in vitro. We examined whether an ISR inhibitor trans-ISRIB (Sidrauski, McGeachy, Ingolia, & Walter, 2015) protects against the EVG-induced OPC maturation defect. Data show that pretreatment with trans-ISRIB 1 hr prior to 3.5 μM EVG exposure allowed differentiation of EVG-treated cells to the level of the controls (Figure 8a-c). By immunoblotting, MBP expression confirmed that trans-ISRIB pretreatment resulted in restoration of MBP expression in EVG-treated cells to the same level as the controls. However, trans-ISRIB did not increase MBP expression after 10 μM EVG treatment (Figure 8d-e). ATF4 expression was examined in the presence and absence of trans-ISRIB pretreatment prior to 10 μM EVG exposure to validate trans-ISRIB as an ISR inhibitor in this model. As expected, data show that ATF4 expression was significantly reduced in cultures pretreated with trans-ISRIB compared with cultures in the absence of trans-ISRIB pretreatment (Figure 8f).

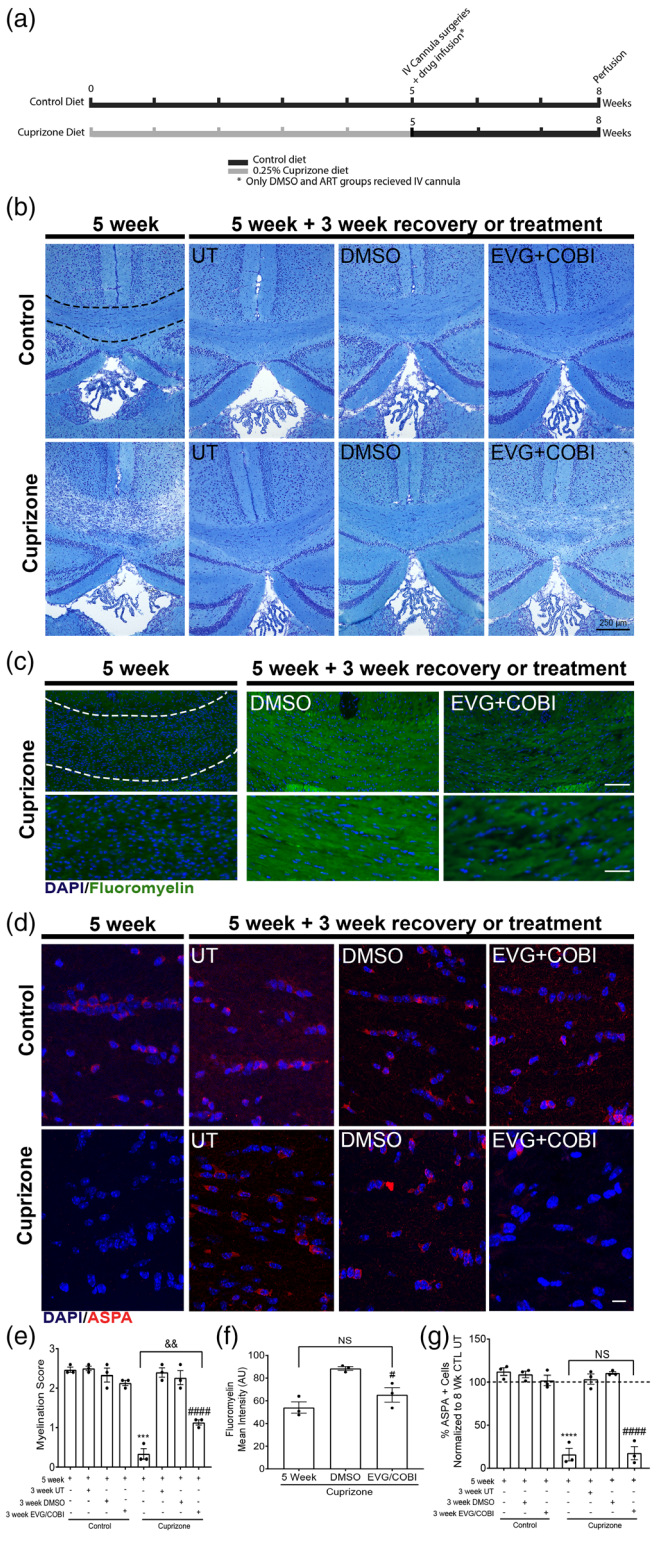

FIGURE 5 EVG inhibits remyelination in vivo following cuprizone-induced demyelination. (a) Schematic of the cuprizone demyelination paradigm. (b) Representative photomicrographs of mouse brain cortical sections stained with luxol fast blue (LFB) for myelin. The dotted lines in 5 week control delineate the corpus callosum; 5 weeks of cuprizone feed lead to intense demyelination of this area; scale bar = 50 μm. (c) Representative photomicrographs of mouse brain cortical sections stained with fluoromyelin green for myelin. Enlargement of photomicrographs included below each panel; scale bar = 50 μm. (d) Representative photomicrographs of mouse corpus callosum stained with mature oligodendrocyte marker ASPA. Cells nuclei are stained with DAPI; scale bar = 50 μm. (e) Semi-quantification of the intensity of demyelination by blind scoring (3 = intact and 0 = complete demyelination). (f) Quantification of fluoromyelin mean staining intensity. (g) Quantification of mature ASPA-positive oligodendrocytes normalized to the number of DAPI-positive cells and expressed as percent of 8 week UT. Data are presented as individual data points (circles) and are expressed as mean ± *SEM* from three animals per group. ***p < .001, ****p < .0001, vs. 5 week control; #p < .05, ####p < .0001, vs. DMSO-injected cuprizone [Color figure can be viewed at wileyonlinelibrary.com]

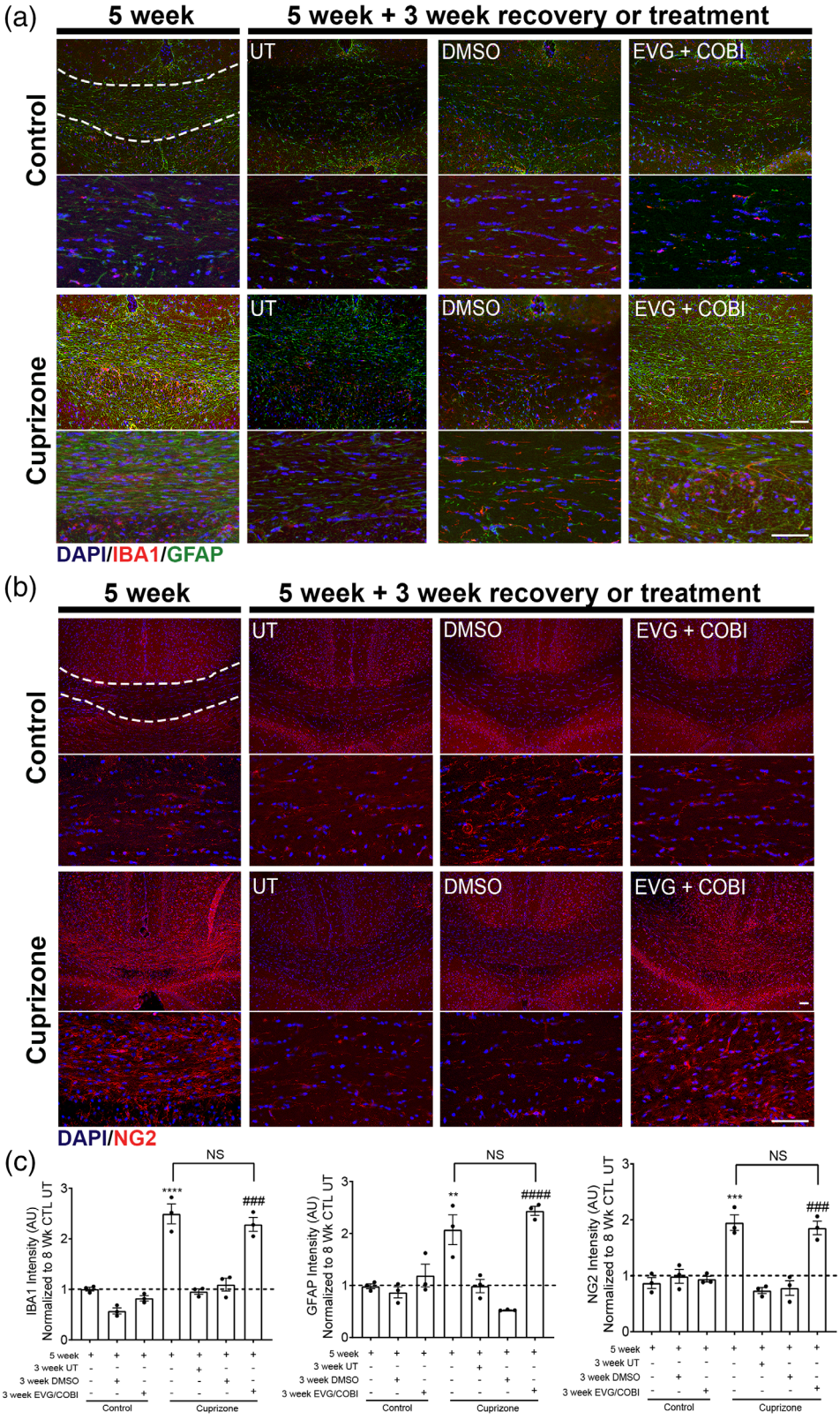

FIGURE 6 Elvitegravir prolongs inflammation following cuprizone-induced demyelination and causes accumulation of OPCs. (a) Representative photomicrographs of mouse brain cortical sections stained with the astrocyte marker GFAP, the microglia marker IBA1 and DAPI. Enlargement of photomicrographs included below each panel; scale bar = 50 μm. The dotted lines in 5 week control delineate the corpus callosum; 5 weeks of cuprizone feed lead to astrogliosis and inflammation of this area, as shown by increased staining intensity for GFAP and IBA1, respectively. (b) Representative photomicrographs of mouse brain cortical sections stained with OPC marker, NG2 and DAPI. Enlargement of photomicrographs included below each panel; scale bar = 50 μm. The dotted lines in 5 week control delineate the corpus callosum; after 5 weeks of cuprizone feed, this area displays increased staining intensity of OPC marker, NG2. (c) Quantification of fluorescent intensities of GFAP, IBA1, and NG2-labeled corpus callosum and normalized to the fluorescent intensity of 8 week UT. Data are presented as individual data points (circles) and are expressed as mean ± *SEM* for three animals per group. $^{**}p < .01$, $^{***}p < .001$, $^{****}p < .0001$ vs. 5 week control; $\#\#\#p < .001$, $\#\#\#\#p < .0001$ vs. DMSO-injected cuprizone [Color figure can be viewed at wileyonlinelibrary.com]

4 | DISCUSSION

The introduction of cART has changed the HIV/AIDS clinical landscape since fewer patients progress to AIDS as a result of efficient viral suppression, thus extending the lifespan of people living with HIV to match uninfected individuals. However, given the persistence of HAND despite cART adherence, a better understanding of neurologic effects of cART is warranted because patients remain on these regimens for the duration of their lives. In this study, we have examined the effects of two ARV compounds from the INSTI class, EVG

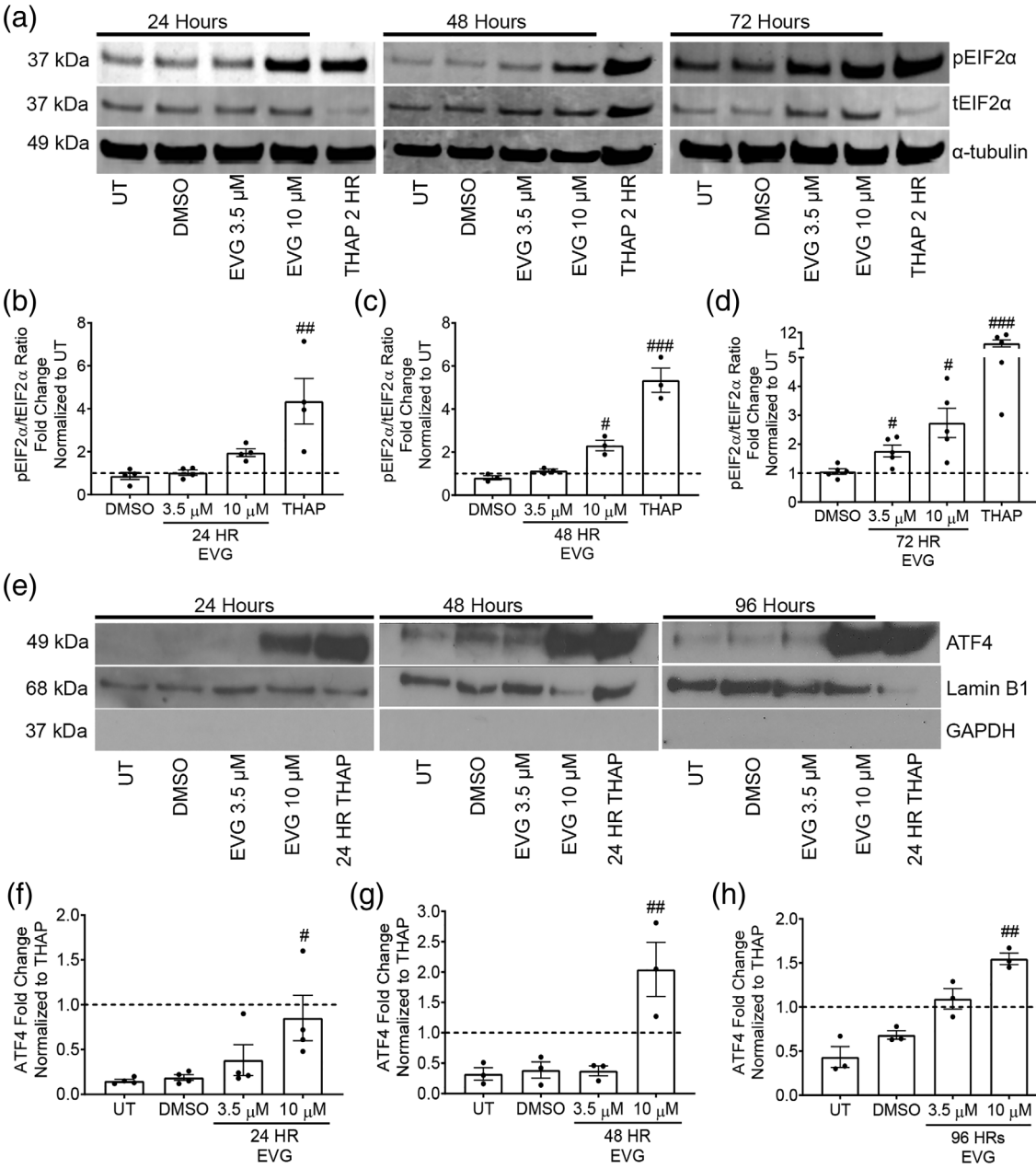

FIGURE 7 EVG activates ISR in cultured oligodendrocytes. Representative western blot images (a) and quantifications of band intensities of pEIF2α and tEIF2α immunoreactivities from cultured oligodendrocytes exposed to 3.5 or 10 μM EVG for (b) 24, (c) 48, and (d) 72 hr. Thapsigargin (THAP) is used as a positive control, always collected at 2 hr posttreatment. Graph data are expressed as mean ± *SEM* from three to five independently prepared cultures. Protein band intensities presented as pEIF2α/tEIF2α ratio and normalized to loading control, α-tubulin are expressed as fold change of UT. #*p* < .05, ##*p* < .01, ###*p* < .001 vs. DMSO. Representative western blot images (e) and quantifications of band intensities of nuclear ATF4 immunoreactivity from cultured oligodendrocytes exposed to 3.5 or 10 μM EVG for (f) 24, (g) 48, and (h) 96 hr with Lamin B1 (present in the nuclear fraction) and GAPDH (present in the cytosolic fraction) as loading controls. No GAPDH band is seen in the nuclear fraction, as expected. THAP is used as a positive control, always collected at 24 hr posttreatment. Graph data are expressed as mean ± *SEM* from three to five independently prepared cultures. Protein bands normalized to Lamin B1 are expressed as fold change of THAP since there was no expression of nuclear ATF4 in UT. #*p* < .05, ##*p* < .01, ###*p* < .001 vs. DMSO

and RAL, since they are widely prescribed as frontline therapy both in the United States and internationally (AIDSinfo, 2019; WHO, 2016). We used our well-established model of primary rat OPC cultures to study the effects of these compounds. We demonstrate that EVG, but not RAL, inhibited oligodendrocyte maturation in vitro and remyelination in vivo. Furthermore, our in vitro findings indicate that the effect of EVG on oligodendrocyte maturation was concentration-dependent, reversible and could be blocked by a specific inhibitor of the ISR. Together with our previous studies demonstrating that ARV compounds from the protease inhibitor class also impaired

oligodendrocyte differentiation (Festa et al., 2019; Jensen et al., 2015), the present work strengthens the possibility that cART may contribute to persistence of white matter pathologies observed in HAND patients.

EVG and RAL concentrations used in vitro were selected to cover a range relevant to the amount of drug observed in patient plasma and CSF (Deeks, 2014; Podany et al., 2017; Yilmaz et al., 2009). Mass spectrometry confirmed that drug levels in the plasma of mice were

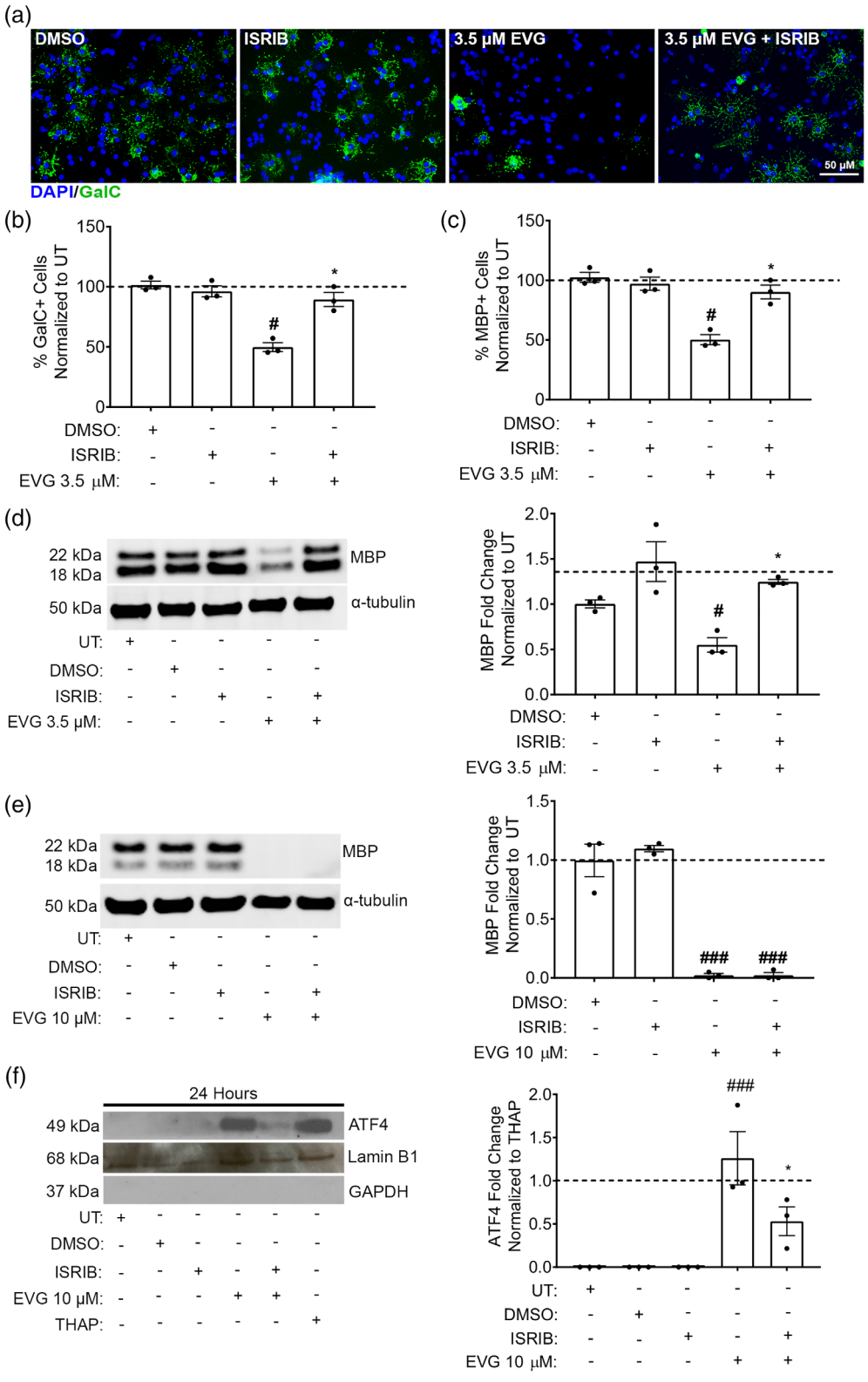

FIGURE 8 Legend on next page.

comparable to that of patients' plasma. It is still unclear how these concentrations relate to acute levels of ARV drugs penetrating the brain parenchyma since some studies have shown that CSF drug concentrations may not accurately reflect amounts in the brain (Anthonypillai, Sanderson, Gibbs, & Thomas, 2004). The current development of new ARV agents with improved CNS penetrance will necessitate a better understanding of their effects in the brain.

Despite both being INSTIs, only EVG caused concentration-dependent inhibition of oligodendrocyte maturation whereas RAL did not. Interestingly, Stern et al., 2018 also showed that only EVG caused neuronal cell death in primary rat cortical cultures whereas RAL did not. It is possible that differences in their physiochemical properties resulted in disparate cellular uptake, intracellular interactions and/or metabolism since RAL is hydrophilic while EVG is lipophilic. In fact, this within-class difference is not uncommon and was also reported for protease inhibitors (Caron, Auclair, Sterlingot, Kornprobst, & Capeau, 2003; Stern et al., 2018). Our findings highlight the existence of critical differences within drug classes and how they may affect oligodendrocyte maturation.

We employed the cuprizone demyelination model in mice to examine the effects of EVG on remyelination in vivo. Cuprizone-induced demyelination is not caused directly by inflammation and leads to the specific degeneration of oligodendrocytes in the corpus callosum (Matsushima & Morell, 2001). Using this model, LFB and fluoromyelin staining showed that daily administration of EVG, during the 3 week recovery period, prevented proper remyelination. Interestingly, there was no gross change in myelin in EVG-injected control mice suggesting that EVG has a more potent effect on the ability of OPCs to remyelinate a demyelinated region but does not cause frank demyelination directly. However, these data should be interpreted with caution since cuprizone-induced demyelination does not reproduce the white matter loss and abnormalities observed in HAND patients. In fact, it has been difficult to reproduce the white matter damage caused by HIV in a typical animal model since the virus itself is species-limited to humans. Nevertheless, both a humanized HIV mouse and the HIV-1 transgenic rat models have shown white matter changes including decreased myelin proteins in the corpus callosum and hippocampus and demyelination (Boska et al., 2014; Lentz et al., 2014). Whether ARV compound administration in these animal models would exacerbate these deficits may be worth examining considering our recent findings.

Our in vivo model suggests that EVG inhibits oligodendrocyte differentiation at a critical time when remyelination should occur, such as following an injury. Indeed, we observed a decreased number of ASPA-positive, differentiated oligodendrocytes in the corpus callosum of EVG-injected cuprizone animals compared with control animals. This correlated with a dramatic loss of myelin as demonstrated by much weaker luxol fast blue and fluoromyelin staining. Furthermore, the accumulation of OPCs at the lesion site, as determined by increased NG2 staining intensity in EVG-injected cuprizone mice, indicates that OPCs are present but are prevented from differentiating into mature oligodendrocytes. The accumulation of OPCs around lesioned areas is often seen in demyelinating diseases such as multiple sclerosis (Nait-Oumesmar et al., 2007). Our studies suggest further investigation into the effects of ARV compounds on white matter are warranted in a clinical setting to help clinicians devise effective drug regimens for HIV patients while minimizing their neurological impact, especially in younger patients who are still developing myelin and may be on cART for decades.

We have identified the ISR as a mechanism mediating the effect of EVG on oligodendrocyte maturation. ISR activation by different classes of ARV compounds, including INSTIs, has been reported both in vitro in cultured neurons and in neurons and astrocytes of HAND patients (Akay et al., 2012; Gannon et al., 2017; Lindl et al., 2007; Stern et al., 2018). Furthermore, there is evidence that the ISR is activated in oligodendrocytes in other neuroinflammatory disease models such as multiple sclerosis (Clayton & Popko, 2016; Romero-Ramírez et al., 2017). Our results suggest that the ISR is activated in oligodendrocytes exposed to EVG, and that the kinetics of its activation are faster with the higher concentration of EVG. Likewise, ATF4 induction was detectable early on in 10 μM EVG-treated cultures but was not significantly increased in 3.5 μM EVG-treated cultures. Cells pretreated with the ISR inhibitor trans-ISRIB were protected only in 3.5 μM EVG-treated cultures and differentiated normally. Furthermore, while the inhibition of differentiation and myelin protein expression caused by 3.5 μM EVG could be reversed by washout of the drug, that of 10 μM EVG took longer to recover and only partially.

FIGURE 8 The ISR inhibitor trans-ISRIB prevents EVG-driven inhibition of oligodendrocyte maturation. (a) Representative photomicrographs of primary rat oligodendrocyte cultures grown in differentiation medium, pretreated with trans-ISRIB for 1 hr prior to EVG exposure for 72 hr, and stained for GalC and DAPI; scale bar = 50 μm. (b) Quantification of GalC-positive immature oligodendrocytes normalized to the number of DAPI-positive cells and expressed as percent of untreated (UT). (c) Quantification of MBP-positive mature oligodendrocytes normalized to the number of DAPI-positive cells and expressed as a percent of UT. #$p < .05$ vs. DMSO. (d, e) Representative western blot images and quantifications of band intensities of MBP immunoreactivity from cultured oligodendrocytes exposed to 3.5 μM (d) or 10 μM (e) EVG for 72 hr with α-tubulin as a loading control. Some cultures were pretreated with trans-ISRIB for 1 hr prior to EVG addition. Graph data are expressed as mean ± *SEM* from three independently prepared cultures. Protein band intensities normalized to α-tubulin are expressed as fold change of UT. ANOVA with Sidak's post hoc. #$p < .05$, ###$p < .001$ vs. DMSO; *$p < .05$, vs. EVG 3.5 μM. (f) Representative western blot image and quantification of band intensities of nuclear ATF4 immunoreactivity from cultured oligodendrocytes exposed to 10 μM EVG for 24 hr with Lamin B1 (present in the nuclear fraction) and GAPDH (present in the cytosolic fraction) as loading controls. Some cultures were pretreated with trans-ISRIB for 1 hr prior to EVG addition. No GAPDH band is seen in the nuclear fraction, as expected. THAP is used as a positive control, always collected at 24 hr posttreatment. Graph data are expressed as mean ± SEM from three independently prepared cultures. Protein bands normalized to Lamin B1 are expressed as fold change of THAP since there was no expression of nuclear ATF4 in UT. ANOVA with Sidak's post hoc. ###$p < .001$ vs. DMSO; *$p < .05$ vs. EVG 10 μM [Color figure can be viewed at wileyonlinelibrary.com]

Taken together, these data suggest that cellular stress elicited by the highest concentration of EVG is irreversible and not surmountable with ISR blockade.

It is also possible that additional mechanisms are triggered that do not respond to trans-ISRIB and that cannot be reversed by removing the drug. For example, we and others have shown that some ARV compounds increased both reactive oxygen species and endolysosomal pH in neurons and oligodendrocytes (Akay et al., 2014; Festa et al., 2019; Hui et al., 2019). The ISR may occur downstream or be concurrent with these other cellular events. Our observation that EVG causes a decrease in MBP *mRNA* levels suggests an effect at the transcriptional or posttranscriptional level prior to protein expression. This indicates that EVG could be affecting transcriptional, epigenetic elements, *mRNA* stability and/or degradation and warrants further investigation.

In summary, our data add to a growing body of evidence suggesting the involvement of cART in the persistence of white matter abnormalities in HAND individuals. We also provide evidence that the ISR pathway mediates, at least in part, the EVG-induced inhibition of oligodendrocyte maturation. In light of this, it is important to consider adjunctive therapies designed not only to alleviate neuronal dysfunctions but also to preserve myelin formation and maintenance.

ACKNOWLEDGMENTS

The authors declare no competing financial interests. This project was supported by the following grants: RO1 MH098742 (KJS and JBG), R21 MH118121 (JBG and KJS) and the Cellular Neuroscience Core of the Institutional Intellectual and Developmental Disabilities Research Core of the Children's Hospital of Philadelphia (HD26979), T32 GM008076 to the Pharmacology Graduate Group at the University of Pennsylvania (LMR) and T32 AI007632 to the Department of Microbiology at the University of Pennsylvania (LF). We thank the NIH AIDS reagent program for their generous donation of ARVs, the laboratory of Michael Robinson, PhD at the Children's Hospital of Philadelphia for the use of the Odyssey Infrared Imaging System, the Mass Spectrometry Core at the Children's Hospital of Philadelphia, Steven Scherer, MD, PhD and Jeff Golden, MD for their helpful suggestions.

DATA AVAILABILITY STATEMENT

The data that support the findings of this study are available from the corresponding author, Judith B. Grinspan, upon reasonable request.

ORCID

Lindsay M. Roth https://orcid.org/0000-0001-6452-3386
Judith B. Grinspan https://orcid.org/0000-0003-0940-5314

REFERENCES

AIDSinfo 2019. Panel on Antiretroviral Guidelines for Adults and Adolescents. Guidelines for the Use of Antiretroviral Agents in Adults and Adolescents with HIV. Department of Health and Human Services. Available at http://www.aidsinfo.nih.govContentFiles/AdultandAdolescentGL.pdf. Accessed [February 17, 2020] [G-4, Table 6a,b]

Akay, C., Cooper, M., Odeleye, A., Jensen, B. K., White, M. G., Vassoler, F., et. al., (2014). Antiretroviral drugs induce oxidative stress and neuronal damage in the central nervous system. *Journal of Neurovirology*, *20*(1), 39–53. https://doi.org/10.1007/s13365-013-0227-1

Akay, C, Lindl, K., Shyam, N., Nabet, B., Goenaga-Vazquez, Y., Ruzbarsky, J., et. al., (2012). Activation status of integrated stress response pathways in neurones and astrocytes of HIV-associated neurocognitive disorders (HAND) cortex. *Neuropathology and Applied Neurobiology*, *38*(2), 175–200. https://doi.org/10.1111/j.1365-2990.2011.01215.x

Anthonypillai, C., Sanderson R. N., Gibbs, J. E., & Thomas, S. A. (2004). The distribution of the HIV protease inhibitor, ritonavir, to the brain, cerebrospinal fluid, and choroid plexuses of the Guinea pig. *Journal of Pharmacology and Experimental Therapeutics*, *308*(3), 912–920. https://doi.org/10.1124/jpet.103.060210

Arts, E., & Hazuda, D. (2012). HIV-1 antiretroviral drug therapy. *Cold Spring Harbor Perspectives in Medicine*, *2*(4), a007161–a007161. https://doi.org/10.1101/cshperspect.a007161

Borjabad, A., Morgello, S., Chao, W., Kim, S.-Y. Y., Brooks, A. I., Murray, J., et. al., (2011). Significant effects of antiretroviral therapy on global gene expression in brain tissues of patients with HIV-1-associated neurocognitive disorders. *PLoS Pathogens*, *7*(9), 1–18. https://doi.org/10.1371/journal.ppat.1002213

Boska, M. D., Dash, P. K., Knibbe, J., Epstein, A. A., Akhter, S. P., Fields, N., et. al., (2014). Associations between brain microstructures, metabolites, and cognitive deficits during chronic HIV-1 infection of humanized mice. *Molecular Neurodegeneration*, *9*(1), 58. https://doi.org/10.1186/1750-1326-9-58

Caron, M., Auclair, M., Sterlingot, H., Kornprobst, M., & Capeau, J. (2003). Some HIV protease inhibitors alter Lamin a/C maturation and stability, SREBP-1 nuclear localization and adipocyte differentiation. *Aids*, *17*(17), 2437–2444. https://doi.org/10.1097/00002030-200311210-00005

Chen, M. F., Gill, A. J., & Kolson, D. L. (2014). Neuropathogenesis of HIV-associated neurocognitive disorders: Roles for immune activation, HIV blipping and viral tropism. *Current Opinion in HIV and AIDS*, *9*(6), 559–564. https://doi.org/10.1097/COH.0000000000000105

Clayton, B., & Popko, B. (2016). Endoplasmic reticulum stress and the unfolded protein response in disorders of myelinating glia. *Brain Research*, *1648*(Pt B), 594–602. https://doi.org/10.1016/j.brainres.2016.03.046

Deeks, E. D. (2014). Elvitegravir: A review of its use in adults with HIV-1 infection. *Drugs*, *74*(6), 687–697. https://doi.org/10.1007/s40265-014-0206-8

Eisenbarth, G. S., Walsh, F. S., & Nirenberg, M. (1979). Monoclonal antibody to a plasma membrane antigen of neurons. *Proceedings of the National Academy of Sciences*, *76*(10), 4913–4917.

Feigenson, K., Reid, M., See, J., Crenshaw, E., & Grinspan, J. B. (2009). Wnt signaling is sufficient to perturb oligodendrocyte maturation. *Molecular and Cellular Neurosciences*, *42*(3), 255–265. https://doi.org/10.1016/j.mcn.2009.07.010

Festa, L., Roth, L. M., Jensen, B. K., Geiger, J. D., Jordan-Sciutto, K. L., & Grinspan, J. B. (2019). Protease inhibitors, Saquinavir and Darunavir, inhibit Oligodendrocyte maturation: Implications for Lysosomal stress. *Journal of Neuroimmune Pharmacology*, 1–12. https://doi.org/10.1007/s11481-019-09893-8

Finzi, D., Hermankova, M., Pierson, T., Carruth, L. M., Buck, C., Chaisson, R. E., et al. (1997). Identification of a reservoir for HIV-1 in patients on highly active antiretroviral therapy. *Science*, *278*(5341), 1295–1300. https://doi.org/10.1126/science.278.5341.1295

Gannon, P. J., Akay-Espinoza, C., Yee, A. C., Briand, L. A., Erickson, M. A., Gelman, B. B., et al. (2017). HIV protease inhibitors Alter amyloid precursor protein processing via β-site amyloid precursor protein cleaving Enzyme-1 translational up-regulation. *The American Journal of Pathology*, *187*(1), 91–109. https://doi.org/10.1016/j.ajpath.2016.09.006

Gavrieli, Y., Sherman, Y., & Ben-Sasson, S. (1992). Identification of programmed cell death in situ via specific labeling of nuclear DNA fragmentation. *The Journal of Cell Biology*, *119*(3), 493–501.

Heaton, R. K., Franklin, D. R., Ellis, R. J., McCutchan, J., Letendre, S. L., Leblanc, S., et. al., (2011). HIV-associated neurocognitive disorders before and during the era of combination antiretroviral therapy: Differences in rates, nature, and predictors. *Journal of Neurovirology*, *17* (1), 3–16. https://doi.org/10.1007/s13365-010-0006-1

Hui, L., Ye, Y., Soliman, M. L., Lakpa, K. L., Miller, N. M., Afghah, Z., et. al., (2019). Antiretroviral drugs promote Amyloidogenesis by De-acidifying Endolysosomes. *Journal of Neuroimmune Pharmacology*, 1–10. https://doi.org/10.1007/s11481-019-09862-1

Jensen, B. K., Monnerie, H., Mannell, M. V., Gannon, P. J., Espinoza, C. A., Erickson, M. A., et. al., (2015). Altered Oligodendrocyte maturation and myelin maintenance: The role of Antiretrovirals in HIV-associated neurocognitive disorders. *Journal of Neuropathology and Experimental Neurology*, *74*(11), 1093–1118. https://doi.org/10.1097/NEN.0000000000000255

Jernigan, T. L., Archibald, S. L., Fennema-Notestine, C., Taylor, M. J., Theilmann, R. J., Julaton, M. D., et. al., (2011). Clinical factors related to brain structure in HIV: The CHARTER study. *Journal of Neurovirology*, *17*(3), 248–257. https://doi.org/10.1007/s13365-011-0032-7

Lentz, M. R., Peterson, K. L., Ibrahim, W. G., Lee, D. E., Sarlls, J., Lizak, M. J., et. al., (2014). Diffusion tensor and volumetric magnetic resonance measures as biomarkers of brain damage in a small animal model of HIV. *PLoS ONE*, *9*(8), 1–8. https://doi.org/10.1371/journal.pone.0105752

Lindl, K., Akay, C., Wang, Y., White, M., & Jordan-Sciutto, K. (2007). Expression of the endoplasmic reticulum stress response marker, BiP, in the central nervous system of HIV-positive individuals. *Neuropathology and Applied Neurobiology*, *33*(6), 658–669. https://doi.org/10.1111/j.1365-2990.2007.00866.x

Madhavarao, C. N., Moffett, J. R., Moore, R. A., Viola, R. E., Namboodiri, M., & Jacobowitz, D. M. (2004). Immunohistochemical localization of aspartoacylase in the rat central nervous system. *The Journal of Comparative Neurology*, *472*(3), 318–329. https://doi.org/10.1002/cne.20080

Matsushima, G., & Morell, P. (2001). The neurotoxicant, cuprizone, as a model to study demyelination and remyelination in the central nervous system. *Brain Pathology (Zurich, Switzerland)*, *11*(1), 107–116. https://doi.org/10.1111/j.1750-3639.2001.tb00385.x

McCarthy, K., & de Vellis, J. (1980). Preparation of separate astroglial and oligodendroglial cell cultures from rat cerebral tissue. *The Journal of Cell Biology*, *85*(3), 890–902. https://doi.org/10.1083/jcb.85.3.890

Nait-Oumesmar, B., Picard-Riera, N., Kerninon, C., Decker, L., Seilhean, D., Höglinger, G. U., et. al., (2007). Activation of the subventricular zone in multiple sclerosis: Evidence for early glial progenitors. *Proceedings of the National Academy of Sciences of the United States of America*, *104* (11), 4694–4699. https://doi.org/10.1073/pnas.0606835104

Pakos-Zebrucka, K., Koryga, I., Mnich, K., Ljujic, M., Samali, A., & Gorman, A. M. (2016). The integrated stress response. *EMBO Reports*, *17*(10), 1374–1395. https://doi.org/10.15252/embr.201642195

Podany, A. T., Scarsi, K. K., & Fletcher, C. V. (2017). Comparative clinical pharmacokinetics and pharmacodynamics of HIV-1 Integrase Strand transfer inhibitors. *Clinical Pharmacokinetics*, *56*(1), 25–40. https://doi.org/10.1007/s40262-016-0424-1

Pomara, N., Crandall, D. T., Choi, S. J., Johnson, G., & Lim, K. O. (2001). White matter abnormalities in HIV-1 infection: A diffusion tensor imaging study. *Psychiatry Research: Neuroimaging*, *106*(1), 15–24. https://doi.org/10.1016/S0925-4927(00)00082-2

Raff, M. C., Mirsky, R., Fields, K., Nature, L. R., Raff, M. C., & Mirsky, R., (1978). Galactocerebroside is a specific cell-surface antigenic marker for oligodendrocytes in culture. *Nature*, *274*(5673), 813–816. http://dx.doi.org/10.1038/274813a0.

Robertson, K., Liner, J., & Meeker, R. B. (2012). Antiretroviral neurotoxicity. *Journal of Neurovirology*, *18*(5), 388–399. https://doi.org/10.1007/s13365-012-0120-3

Romero-Ramírez, L., Nieto-Sampedro, M., & Barreda-Manso, A. M. (2017). Integrated stress response as a therapeutic target for CNS injuries. *BioMed Research International*, *2017*, 1–7. https://doi.org/10.1155/2017/6953156

Saylor, D., Dickens, A., Sacktor, N., Haughey, N., Slusher, B., Pletnikov, M., et al. (2016). HIV-associated neurocognitive disorder—pathogenesis and prospects for treatment. *Nature Reviews. Neurology*, *12*(4), 234–248. https://doi.org/10.1038/nrneurol.2016.27

Shah, A., Gangwani, M. R., Chaudhari, N. S., Glazyrin, A., Bhat, H. K., & Kumar, A. (2016). Neurotoxicity in the post-HAART era: Caution for the antiretroviral therapeutics. *Neurotoxicity Research*, *30*(4), 677–697. https://doi.org/10.1007/s12640-016-9646-0

Sidrauski, C., McGeachy, A. M., Ingolia, N. T., & Walter, P. (2015). The small molecule ISRIB reverses the effects of eIF2α phosphorylation on translation and stress granule assembly. *eLife*, *4*, e05033. https://doi.org/10.7554/eLife.05033

Solomon, I. H., Chettimada, S., Misra, V., Lorenz, D. R., Gorelick, R. J., Gelman, B. B., et. al., (2019). White matter abnormalities linked to interferon, stress response, and energy metabolism gene expression changes in older HIV-positive patients on antiretroviral therapy. *Molecular Neurobiology*, 1–16. https://doi.org/10.1007/s12035-019-01795-3, *57*

Stern, A. L., Lee, R. N., Panvelker, N., Li, J., Harowitz, J., Jordan-Sciutto, K. L., & Akay-Espinoza, C. (2018). Differential effects of antiretroviral drugs on neurons in vitro: Roles for oxidative stress and integrated stress response. *Journal of Neuroimmune Pharmacology*, *13*(1), 64–76. https://doi.org/10.1007/s11481-017-9761-6

Tate, D. F., Sampat, M., Harezlak, J., Fiecas, M., Hogan, J., Dewey, J., et. al., (2011). Regional areas and widths of the midsagittal corpus callosum among HIV-infected patients on stable antiretroviral therapies. *Journal of Neurovirology*, *17*(4), 368–379. https://doi.org/10.1007/s13365-011-0033-6

Waxman, S. G. (1980). Determinants of conduction velocity in myelinated nerve fibers. *Muscle & Nerve*, *3*(2), 141–150. https://doi.org/10.1002/mus.880030207

Wohlschlaeger, J., Wenger, E., Mehraein, P., & Weis, S. (2009). White matter changes in HIV-1 infected brains: A combined gross anatomical and ultrastructural morphometric investigation of the corpus callosum. *Clinical Neurology and Neurosurgery*, *111*(5), 422–429. https://doi.org/10.1016/j.clineuro.2008.12.006

World Health Organization. (2016). Consolidated Guidelines on the Use of Antiretroviral Drugs for Treating and Preventing HIV Infection: Recommendations for a Public Health Approach. Available at https://apps.who.int/iris/bitstream/handle/10665/208825/9789241549684_eng.pdf?sequence= Accessed [February 17th 2020] [Pages 97–102]

Yilmaz, A., Gisslén, M., Spudich, S., Lee, E., Jayewardene, A., Aweeka, F., & Price, R. W. (2009). Raltegravir cerebrospinal fluid concentrations in HIV-1 infection. *PLoS One*, *4*(9), e6877. https://doi.org/10.1371/journal.pone.0006877

Yin, X., Baek, R. C., Kirschner, D. A., Peterson, A., Fujii, Y., Nave, K.-A., et. al., (2006). Evolution of a neuroprotective function of central nervous system myelin. *The Journal of Cell Biology*, *172*(3), 469–478. https://doi.org/10.1083/jcb.200509174

Yu, Q., Hui, R., Park, J., Huang, Y., Kusnecov, A. W., Dreyfus, C. F., & Zhou, R. (2017). Strain differences in cuprizone induced demyelination. *Cell & Bioscience*, *7*(1), 59. https://doi.org/10.1186/s13578-017-0181-3

How to cite this article: Roth LM, Zidane B, Festa L, et al. Differential effects of integrase strand transfer inhibitors, elvitegravir and raltegravir, on oligodendrocyte maturation: A role for the integrated stress response. *Glia*. 2021;69: 362–376. https://doi.org/10.1002/glia.23902